Investigation on the Suitability of Two-Dimensional Depth-Averaged Models for Bend-Flow Simulation

T. Y. Hsieh[1] and J. C. Yang, M.ASCE[2]

Abstract: A numerical experiment is carried out to study the suitability of two-dimensional (2D) depth-averaged modeling for bend-flow simulation, in which the geometry of the studied channel is rectangular. Two commonly used 2D depth-averaged models for bend-flow simulation are considered in this study of which the bend-flow model includes the dispersion stress terms by incorporating the assumption of secondary-current velocity profile, and the conventional model neglects the dispersion stress terms. The maximum relative discrepancy of the longitudinal velocity, obtained from the comparison of these two models, is used as a criterion to judge their applicability for bend-flow simulation. The analysis of simulation results indicated that the maximum relative difference in longitudinal velocity is mainly related to the relative strength of the secondary current and the relative length of the channel. Empirical relations between the maximum relative difference in the longitudinal velocity, the relative strength of the secondary current, and the relative length of the channel for both the channel-bend region and the straight region following the bend have been established. The proposed relations provide a guideline for model users to determine the proper approach to simulate the bend-flow problem by either using the conventional model or the bend-flow model. Experimental data have been adopted herein to demonstrate the applicability and to verify the accuracy of the proposed relations.

DOI: 10.1061/(ASCE)0733-9429(2003)129:8(597)

CE Database subject headings: Channel bend; Two-dimensional models; Secondary flow; Flow simulation.

Introduction

Flow pattern in curved channels is three-dimensional (3D) and many 3D numerical models have been developed (Leschziner and Rodi 1979; Sinha et al. 1998; Wu et al. 2000; Meselhe and Sotiropoulos 2000) to simulate the complicated spiral flow motion in river bends. However, hydraulic engineers in practice often adopt two-dimensional (2D) depth-averaged models because of their simplicity in implementation and application. The 2D depth-averaged models can be classified into two types: The conventional model and the bend-flow model. The major difference between the two is the treatment of dispersion stress terms in the momentum equations. Integrals along the vertical direction of velocity deviations from the depth-averaged values represent the dispersion stress terms. The conventional model assumes that vertical velocity is uniform and the secondary-current effect is ignored. On the other hand, the bend-flow model takes into account the influence of the dispersion stress terms arisen from the integration of the products of the discrepancy between the mean and the adopted secondary-current velocity distribution.

[1]PhD Candidate, Dept. of Civil Engineering and Hazard Mitigation Research Center, National Chial Tung Univ., 1001 Ta Hsueh Rd., Hsinchu, 30050 Taiwan. E-mail: tyhsieh.cv86g@nctu.edu.tw

[2]Professor, Dept. of Civil Engineering and Hazard Mitigation Research Center, National Chial Tung Univ., 1001 Ta Hsueh Rd., Hsinchu, 30050 Taiwan. E-mail: jcyang@mail.nctu.edu.tw

Note. Discussion open until January 1, 2004. Separate discussions must be submitted for individual papers. To extend the closing date by one month, a written request must be filed with the ASCE Managing Editor. The manuscript for this paper was submitted for review and possible publication on December 27, 2001; approved on February 17, 2003. This paper is part of the ***Journal of Hydraulic Engineering***, Vol. 129, No. 8, August 1, 2003. ©ASCE, ISSN 0733-9429/2003/8-597–612/$18.00.

Conventional models have been widely used by many researchers. Molls and Chaudhry (1995) proposed the concept of the integrated effective stresses, which consists of the laminar viscosity stresses and the turbulent stresses, to simulate the experimental bend-flow data reported by Rozovskii (1961). Ye and McCorquodale (1997) proposed a fractional two-step implicit model to simulate the experimental bend-flow data reported by Chang (1971). Both simulated results showed good agreement as compared with the experimental data.

However, the use of the conventional models for bend-flow simulation have been criticized by a number of investigators (Flokstra 1977; Finnie et al. 1999; Lien et al. 1999a). Flokstra (1977) indicated the need of dispersion stress terms for bend-flow problem. Finnie et al. (1999) later followed Flokstra's concept to solve a transport equation for streamwise vorticity and incorporated the so-called associated acceleration terms, i.e., dispersion stress terms, to the depth-averaged equations. The inclusion of these acceleration terms results in improved predictions of depth-averaged velocity in bend-flow simulation. Lien et al. (1999a) further showed that the simulated results without considering the dispersion stress terms are consistent with the potential theory, in which the velocity distribution is skewed inward and away from the sidewalls and approaches to the free-vortex distribution.

de Vriend (1977), Odgaard (1989), and Yen and Ho (1990) have developed steady bend-flow models to avoid the possible numerical instability and requiring a great amount of computation time. But all of them disregarded the convective influence of the secondary current on the main flow, the de Vriend's so-called secondary convection terms on the main flow. Kalkwijk and de Vriend (1980) developed a steady bend-flow model to simulate the experimental bend-flow data conducted by de Vriend and Koch (1977), in which the convective influence of the secondary current on the main flow is considered. However, they did not

J. Hydraul. Eng. 2003.129:597-612.

consider one of the dispersion stress terms induced by the vertical velocity discrepancy in the transverse direction, which might become the dominant stress in the sharply curved channel (Lien et al. 1999a). Nagata et al. (1997) and Finnie et al. (1999) developed unsteady bend-flow models by ignoring the dispersion stress terms in the transverse direction. Lien et al. (1999a) proposed an unsteady 2D bend-flow model to capture all the effect of dispersion stress terms in the bend-flow simulation.

In the aforementioned studies, there are two categories of the 2D depth-averaged model for bend-flow simulation. The intention of this paper is to establish a guideline for users to select a more appropriate 2D model for bend-flow problems. Lien et al.'s (1999a) concept considering all of the effects of dispersion stress terms in the governing equations is adopted in developing the bend-flow model. The two-step split-operator approach proposed by Lien et al. (1999b) is used to solve the governing equations for both models. The suitability of 2D depth-averaged models in a bend-flow simulation will be analyzed by comparing the calculated velocity and depth from the models. The parameters that influence the suitability of 2D depth-averaged models for a bend-flow simulation will be identified through dimensional analysis. The relationships between the maximum relative difference and key parameters will be established for both the channel-bend region and outlet straight region following the bend. The relationships can provide some guidelines for determining the suitability of 2D depth-averaged models for bend-flow simulation. The experimental data from de Vriend and Koch (1977) is adopted herein for assessing the accuracy and applicability of a model for simulating bend-flow behavior.

Hydrodynamic Model

Mathematical Formulation

The following assumptions are made in the model developed herein: (1) incompressible Newtonian fluid; (2) hydrostatic pressure distribution; (3) negligible wind shear at the water surface; (4) negligible Coriolis acceleration. The governing equations in 3D form are integrated over the depth to obtain the 2D conservative depth-averaged equations in orthogonal curvilinear coordinates as follows: Continuity equation

$$h_1 h_2 \frac{\partial d}{\partial t} + \frac{\partial}{\partial \xi}(h_2 \bar{u} d) + \frac{\partial}{\partial \eta}(h_1 \bar{v} d) = 0 \tag{1}$$

Momentum equations

$$\begin{aligned}
&\frac{\partial \bar{u}}{\partial t} + \frac{\bar{u}}{h_1}\frac{\partial \bar{u}}{\partial \xi} + \frac{\bar{v}}{h_2}\frac{\partial \bar{u}}{\partial \eta} + \frac{1}{h_1 h_2}\frac{\partial h_1}{\partial \eta}\bar{u}\bar{v} - \frac{1}{h_1 h_2}\frac{\partial h_2}{\partial \xi}\bar{v}^2 \\
&= -\frac{g}{h_1}\frac{\partial}{\partial \xi}(z_b + d) + \frac{1}{\rho h_1 h_2 d}\frac{\partial}{\partial \xi}(h_2 T_{11}) \\
&\quad + \frac{1}{\rho h_1 h_2 d}\frac{\partial}{\partial \eta}(h_1 T_{12}) + \frac{1}{\rho h_1 h_2 d}\frac{\partial h_1}{\partial \eta}T_{12} - \frac{1}{\rho h_1 h_2 d}\frac{\partial h_2}{\partial \xi}T_{22} \\
&\quad - \frac{\tau_{b_1}}{\rho d} + \frac{1}{\rho h_1 h_2 d}\left[-(h_2\tau_{11})_s\frac{\partial z_s}{\partial \xi} + (h_2\tau_{11})_b\frac{\partial z_b}{\partial \xi}\right. \\
&\quad \left. - (h_1\tau_{12})_s\frac{\partial z_s}{\partial \eta} + (h_1\tau_{12})_b\frac{\partial z_b}{\partial \eta}\right]
\end{aligned} \tag{2}$$

$$\begin{aligned}
&\frac{\partial \bar{v}}{\partial t} + \frac{\bar{u}}{h_1}\frac{\partial \bar{v}}{\partial \xi} + \frac{\bar{v}}{h_2}\frac{\partial \bar{v}}{\partial \eta} + \frac{1}{h_1 h_2}\frac{\partial h_2}{\partial \xi}\bar{u}\bar{v} - \frac{1}{h_1 h_2}\frac{\partial h_1}{\partial \eta}\bar{u}^2 \\
&= -\frac{g}{h_2}\frac{\partial}{\partial \eta}(z_b + d) + \frac{1}{\rho h_1 h_2 d}\frac{\partial}{\partial \xi}h_1 T_{12} \\
&\quad + \frac{1}{\rho h_1 h_2 d}\frac{\partial}{\partial \eta}h_1 T_{22} - \frac{1}{\rho h_1 h_2 d}\frac{\partial h_1}{\partial \eta}T_{11} + \frac{1}{\rho h_1 h_2 d}\frac{\partial h_2}{\partial \xi}T_{12} \\
&\quad - \frac{\tau_{b_2}}{\rho d} + \frac{1}{\rho h_1 h_2 d}\left[-(h_2\tau_{12})_s\frac{\partial z_s}{\partial \xi} + (h_2\tau_{12})_b\frac{\partial z_b}{\partial \xi}\right. \\
&\quad \left. - (h_1\tau_{22})_s\frac{\partial z_s}{\partial \eta} + (h_1\tau_{22})_b\frac{\partial z_b}{\partial \eta}\right]
\end{aligned} \tag{3}$$

in which

$$\begin{aligned}
T_{11} &= \int_{z_b}^{z_s}[\tau_{11} - \rho\overline{u'^2} - \rho(\bar{u} - \bar{\bar{u}})^2]dz \\
T_{22} &= \int_{z_b}^{z_s}[\tau_{22} - \rho\overline{v'^2} - \rho(\bar{v} - \bar{\bar{v}})^2]dz \\
T_{12} = T_{21} &= \int_{z_b}^{z_s}[\tau_{12} - \rho\overline{u'v'} - \rho(\bar{u} - \bar{\bar{u}})(\bar{v} - \bar{\bar{v}})]dz
\end{aligned} \tag{4}$$

where ξ and η = orthogonal curvilinear coordinates in streamwise axis and transverse axis, respectively; h_1 and h_2 = metric coefficients in ξ and η directions, respectively; u and v = velocity components in ξ and η directions, respectively; ρ = fluid density; g = gravitational acceleration; t = the time; d = depth; z_b = bed elevation; z_s = water surface elevation; overbar ($\bar{}$) = time average; double overbar ($\bar{\bar{}}$) = depth average; prime ($'$) = fluctuating component; and subscripts s and b = the dependent variables at the water surface and channel bed, respectively. The effective stresses (T_{11}, T_{12}, T_{22}) consist of laminar viscous stresses, turbulent stresses, and dispersion stresses due to depth-averaged operations.

Closure Model—Quantifying Stress Terms

To solve Eqs. (1)–(3) as a closed system, the stress terms on the right-hand side of Eqs. (2) and (3) have to be expressed as explicit functions of the depth-averaged velocity and the depth.

The bottom shear stresses τ_{b1}, τ_{b2} are modeled according to the following formulas (Rastogi and Rodi 1978)

$$\tau_{b_1} = C_f \rho \bar{u}(\bar{u}^2 + \bar{v}^2)^{1/2}, \quad \tau_{b_2} = C_f \rho \bar{v}(\bar{u}^2 + \bar{v}^2)^{1/2} \tag{5}$$

where $C_f = g/c^2$ = friction factor; and c = Chezy factor.

The laminar viscous stresses and turbulent stresses can be quantified in accordance with the Boussinesq eddy-viscosity concept, which can be expressed as

$$\begin{aligned}
\frac{\tau_{11}}{\rho} - \overline{u'^2} &= 2\nu\left[\frac{1}{h_1}\frac{\partial \bar{u}}{\partial \xi} + \frac{\bar{v}}{h_1 h_2}\frac{\partial h_1}{\partial \eta}\right] \\
\frac{\tau_{22}}{\rho} - \overline{v'^2} &= 2\nu\left[\frac{1}{h_2}\frac{\partial \bar{v}}{\partial \eta} + \frac{\bar{u}}{h_1 h_2}\frac{\partial h_2}{\partial \xi}\right] \\
\frac{\tau_{12}}{\rho} - \overline{u'v'} &= 2\nu\left[\frac{h_2}{h_1}\frac{\partial}{\partial \xi}\left(\frac{\bar{v}}{h_2}\right) + \frac{h_1}{h_2}\frac{\partial}{\partial \eta}\left(\frac{\bar{u}}{h_1}\right)\right]
\end{aligned} \tag{6}$$

J. Hydraul. Eng. 2003.129:597-612.

where $\nu=\nu_l+\nu_t$; ν_l=laminar kinematic viscosity; ν_t=turbulent kinematic viscosity=$ku_*d/6$ (Falcon 1979); $u_*=(\tau_b/\rho)^{1/2}$=shear velocity; and k=von Karman's constant (about 0.4).

The dispersion stresses are evaluated explicitly, using assumed shape functions for the velocity profile. However, it is almost impossible to have a global analytical velocity profile which is suitable for any kind of bend-flow field. In general, the vertical velocity distribution used in the bend-flow model is under the assumptions of single secondary eddy and developed flow. As far as the modeling development is concerned, many researchers (de Vriend and Geldof 1983; Odgaard 1989; Lien et al. 1999a) have pointed out that the use of the velocity profile with these assumptions should be appropriate.

The velocity profiles in the streamwise and transverse directions proposed by de Vriend (1977) are adopted in the bend-flow model:

$$\bar{u}=\bar{\bar{u}}\left[1+\frac{\sqrt{g}}{kc}+\frac{\sqrt{g}}{kc}\ln\zeta\right]=\bar{\bar{u}}f_m(\zeta) \tag{7}$$

$$\bar{v}=\bar{\bar{v}}f_m(\zeta)+\frac{\bar{\bar{u}}d}{k^2r}\left[2F_1(\zeta)+\frac{\sqrt{g}}{kc}F_2(\zeta)-2\left(1-\frac{\sqrt{g}}{kc}\right)f_m(\zeta)\right] \tag{8}$$

in which

$$F_1(\zeta)=\int_0^1\frac{\ln\zeta}{\zeta-1}d\zeta,\quad F_2(\zeta)=\int_0^1\frac{\ln^2\zeta}{\zeta-1}d\zeta \tag{9}$$

where $\zeta=(z-z_b)/d$=dimensionless distance from the bed; and r=radius of curvature.

The use of the de Vriend's (1977) profile requires the following assumptions: (1) the depth is small compared with the width (shallow channel); (2) the width is small compared with the radius of curvature (not too sharply curved channel); (3) single secondary eddy only; and (4) developed flow.

Numerical Methodology

The two-step split-operator algorithm proposed by Lien et al. (1999b) is used in the present study. The first step (dispersion process) is to compute the provisional velocity in the momentum equation without considering the pressure gradient and bed friction. The second step (propagation process) is to correct the provisional velocity by considering the effect of the pressure gradient and bed friction. The framework of the algorithm can be expressed as following:

First step: dispersion process$\Rightarrow\bar{\bar{u}}^{n+1/2}$, $\bar{\bar{v}}^{n+1/2}$

Second step: propagation process$\Rightarrow d^{n+1}$, $\bar{\bar{u}}^{n+1}$, $\bar{\bar{v}}^{n+1}$

where the superscript $n+1$ refers to the time level $(n+1)\Delta t$; and the superscript $n+1/2$ denotes the intermediate step between n and $n+1$.

The dispersion step includes convection and diffusion terms. In order to catch the flow direction, a simple hybrid scheme is used for convection terms. Diffusion terms are discretized using the concept of control volume. Coupled with convection and diffusion terms, the ADI scheme is adopted to solve the discretization equations. The propagation step includes pressure, gravity, and bottom shear stresses terms, and none of velocity gradient appears in this step. The propagation step can be discretized into a simple algebraic equation while the unknown can be solved directly. Similar to the diffusion terms, the continuity equation is discretized by using the concept of control volume and solved by the ADI scheme.

Boundary Conditions

Three types of boundaries, namely, the inlet, outlet, and solid walls are considered. Discharge hydrograph per unit width can be specified along the inlet section. Water surface elevation can be specified along the outlet section. At the solid boundaries, the law of the wall is applied outside the viscous sublayer and transition layer. The wall shear stress is used as the wall boundary condition and is substituted into the momentum equation in the wall region to solve for the velocity component parallel to the wall.

Dimensional Analysis

By comparing the results of velocity and depth from the bend-flow model and the conventional model, one can determine the applicability of the model for a bend-flow simulation. To conduct the model comparison study, the maximum relative difference, $\mathrm{Max}(\Delta\Psi/\Psi^b)$, is used as an index to distinguish the applicable constraints of models; in which Ψ could stand for $\bar{u}$, or $\bar{v}$, or d at each grid point except the wall region in which the wall shear stress is used; $\Delta\Psi$ represents the difference of Ψ between models; Ψ^b denotes the result from the bend-flow model which is used herein as the reference for comparison; and Max represents the maximum value for the case compared.

In order to seek the physically meaningful parameters related to the maximum relative differences in velocity and depth between the bend-flow model and the conventional model, the dimensional analysis is performed. Major factors that influence the characteristics of the flow in a curved channel can be categorized into three groups (Yen 1965) which include the fluid properties, the hydraulic characteristics of the channel, and the sediment properties. The fluid properties include fluid density ρ and viscosity μ. The hydraulic characteristics of the channel includes mean velocity U and V, mean flow depth H, channel width B, channel length L, centerline radius of curvature r_c, channel slope S_0, gravitational acceleration g, and the parameters which describe the shape of the cross section. In the present study, the rectangular cross section with single bend was considered. The flow is clear water, and the movable bed is replaced by a surface of specific roughness. The functional relationship can be described as

$$\mathrm{Max}U^*,\mathrm{Max}V^*,\mathrm{Max}H^*=f_1(\rho,\mu,g,L,U,V,H,B,r_c,S_0,c) \tag{10}$$

in which $\mathrm{Max}U^*=\mathrm{Max}(|\Delta\bar{u}|/\bar{u}^b)$=maximum relative difference in longitudinal velocity; $\mathrm{Max}V^*=\mathrm{Max}(|\Delta\bar{v}|/\bar{v}^b)$=maximum relative difference in transverse velocity; $\mathrm{Max}H^*=\mathrm{Max}(|\Delta d|/d^b)$=maximum relative difference in depth; $\Delta\bar{u}$=difference in longitudinal velocity between models; $\Delta\bar{v}$=difference in transverse velocity between models; Δd=difference in depth between models; $\bar{u}^b$=longitudinal velocity from the bend-flow model; $\bar{v}^b$=transverse velocity from the bend-flow model; d^b=depth from the bend-flow model; $c=R^{1/6}/n$; n=Manning's roughness coefficient; and R=hydraulic radius.

The use of orthogonal curvilinear coordinates system will remove the effects of $\Delta\bar{v}$ and V. Hence, for the rest of ten independent variables, one can obtain seven independent dimensionless parameters, according to Vaschy-Buckingham's theorem, as follows:

J. Hydraul. Eng. 2003.129:597-612.

Table 1. Simulated Data

Case No.	Unit discharge ($m^3/s/m$)	Width (m)	Bend radius (m)	Slope ($\times 10^{-3}$)	Chezy factor ($m^{1/2}/s$)
1–67	0.0167–0.6667	3,6,9,12,15	50	1.0	30
68–133	0.0167–0.6667	6,15	25,75,100,125,150	1.0	30
134–212	0.0042–0.8001	6	50	0.1, 0.5, 2.5, 5.0, 7.5, 10.0	30
213–289	0.0050–0.6667	6	50	1.0	10,20,40,50,60,70

$$\mathsf{R}=\rho UH/\mu, \quad \mathsf{F}=U/\sqrt{gH}, \quad \theta=L/(2\pi r_c)$$
$$SI=UH/(u_* r_c)=H/(r_c\sqrt{C_f}), \quad H/B, \quad S_0, \quad C_f=g/c^2 \tag{11}$$

in which R = Reynolds number; F = Froude number; θ = relative length of channel; SI = relative strength of secondary current; H/B = depth–width ratio; S_0 = channel slope; C_f = friction factor; and $u_* = \sqrt{C_f}U$ = shear velocity.

Based on the dimensionless parameters, a general functional relation may be expressed as

$$\text{Max}U^*, \text{Max}H^* = f_2(\mathsf{R}, \mathsf{F}, \theta, SI, H/B, S_0, C_f) \tag{12}$$

The MaxU^* and MaxH^* will be used as criteria to judge whether a given bend has significant momentum exchange due to secondary current, and whether the bend-flow problem can be solved properly by a 2D depth-averaged model.

Case Setup

To investigate the effects of the dimensionless parameters in Eq. (12) on MaxU^* and MaxH^*, a number of hypothetical cases in compliance with the assumptions of de Vriend's (1977) profile, namely, shallow depth and not too sharply curved channels, were analyzed. Therefore, in the present study, the depth–width ratio and the width–radius ratio for all cases are restricted to be less than 0.1. Manning's n varied between 0.01 and 0.1. Specifically, data sets were generated under the following conditions: The depth–width ratio varied between 4.5×10^{-3} and 9.41×10^{-2}; depth–radius ratio varied between 4.5×10^{-4} and 4.2×10^{-2}; and the friction factor varied between 2.0×10^{-3} and 9.81×10^{-2}.

The channel considered has rectangular geometry and has a 90° single bend. The bend is connected to a 10 m long inlet reach and a 10 m long outlet reach with the same cross section as the bend to avoid the boundary effect.

In generating the test case, each data set has only one variable varied while the rest of variables are fixed. All data sets generated can be categorized into four groups as shown in Table 1.

The number of cases designed is 289 in total. The data sets covered a wide range of possible flow conditions satisfying the assumptions of de Vriend's profile. R varied between 2.74×10^3 and 5.27×10^5; F between 0.088 and 0.942; SI between 0.004 and 0.409. The relative length of the bend θ_b ($\theta_b = L_b/(2\pi r_c)$; L_b = the bend length measured from the bend entrance along the channel centerline) varied between 0 and 0.25. The relative length of the outlet straight channel θ_{os} ($\theta_{os} = L_{os}/(2\pi r_c)$; L_{os} = the outlet straight channel length measured from the bend exit along the channel centerline) varied between 0 and 0.0637.

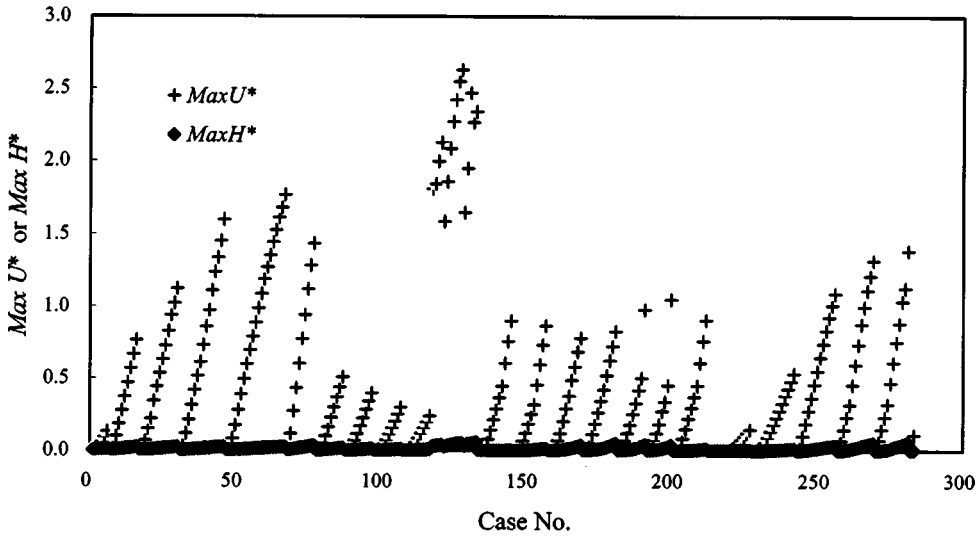

Fig. 1. Variation of MaxH^* and MaxU^* for simulated cases

Table 2. Regression Coefficients of MaxU^* versus Dimensionless Parameters in Channel-bend Region

Factor	ln(SI)	ln(R)	ln(C_f)	ln(F)	ln(θ_b)	ln(S_0)	ln(H/B)	R^2
Coefficient	1.77	0.115	6.29	12.4	0.341	−6.16	1.20	93.8%

J. Hydraul. Eng. 2003.129:597-612.

Table 3. Regression Coefficients of MaxU^* versus Dimensionless Parameters in Channel-bend Region

Factor	ln(SI)	ln(R)	ln(C_f)	ln(θ_b)	ln(S_0)	R^2
Coefficient	2.16	0.21	0.30	0.34	0.06	90.4%

Note: F and H/B ignored.

In each case, the steady unit discharge was specified along the inlet section as the upstream boundary condition; the normal depth of flow was specified at the outlet section as the downstream boundary condition. The grid sizes selected are fine enough to ensure that the simulated results are grid independent. With regard to the convergence of the model, the following cri-

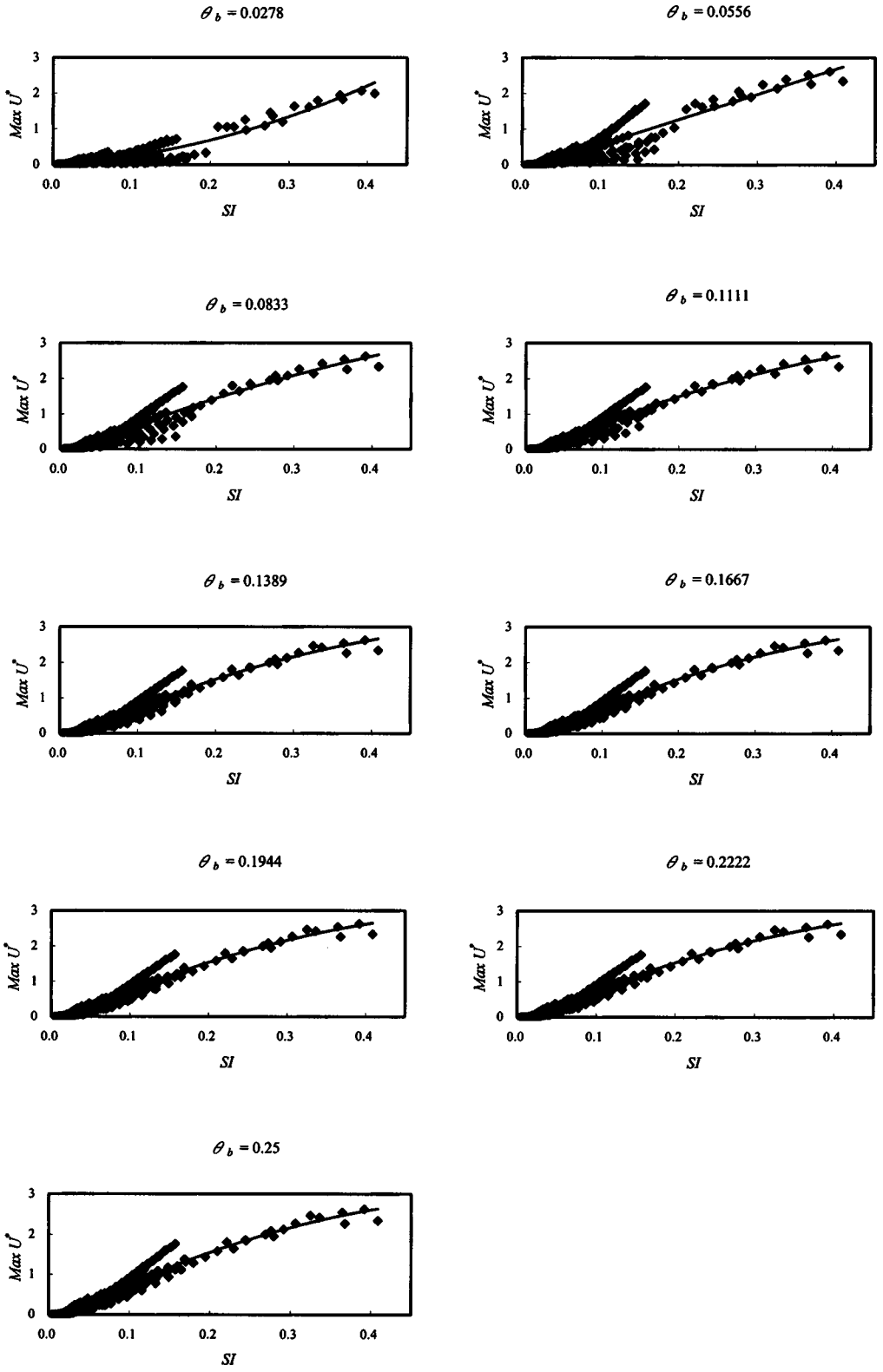

Fig. 2. MaxU^* as function of SI for various θ_b

J. Hydraul. Eng. 2003.129:597-612.

Table 4. Regression Functions of MaxU^* versus SI for Various θ_b

θ_b	Regression functions	R^2
0.0278	$\text{Max}U^* = 10.581SI^2 + 1.3102SI - 0.0012$	0.890
0.0556	$\text{Max}U^* = 0.2329SI^2 + 6.9466SI - 0.133$	0.855
0.0833	$\text{Max}U^* = -5.6052SI^2 + 9.2925SI - 0.1908$	0.900
0.1111	$\text{Max}U^* = -7.5538SI^2 + 10.067SI - 0.212$	0.927
0.1389	$\text{Max}U^* = -7.979SI^2 + 10.314SI - 0.2191$	0.937
0.1667	$\text{Max}U^* = -8.3139SI^2 + 10.44SI - 0.2222$	0.941
0.1944	$\text{Max}U^* = -8.5011SI^2 + 10.511SI - 0.2242$	0.943
0.2222	$\text{Max}U^* = -8.6154SI^2 + 10.552SI - 0.2246$	0.944
0.25	$\text{Max}U^* = -8.9197SI^2 + 10.629SI - 0.2192$	0.943

teria should be satisfied:

$$\max[(\Psi_{i,j}^{n+1} - \Psi_{i,j}^{n})/\Psi_{i,j}^{n}] \leqslant 1.0 \times 10^{-5} \tag{13}$$

where Ψ could stand for $\bar{u}$, or $\bar{v}$, or d at each grid point.

Parametric Analyses

As pointed out by Nouh and Townsend (1979), the secondary current associated with the flow in a channel bend is generated at the entrance to the bend, reaches its maximum strength within the bend section, and has a negligible effect after a limited distance along the straight channel after exiting the bend. Hence, the flow in a single bend can be classified into three regions, namely, (1) inlet straight region before the entrance to the bend; (2) channel-bend region; and (3) outlet straight region following the bend.

In the straight portions of the channel in which the radius of curvature tends to be infinity, the dispersion stress terms can be neglected. Therefore, in region 1, both the conventional and the bend-flow models should give the same results. Nevertheless, the secondary-current effect will be activated due to the bend curvature in region 2, and will last for a certain distance in region 3. Therefore, the suitability of both models for bend-flow simulation can be distinguished through the analysis of the relative maximum difference, i.e., Eq. (12), for regions 2 and 3. The analyses for these two regions will be given, respectively, in the following.

Flow in Channel Bends

The MaxU^* and MaxH^* of each case in the entire channel-bend region are shown in Fig. 1. From Fig. 1, one can observe that the values of MaxH^* are smaller than 6% and always much smaller than MaxU^* for all of the cases simulated. This is because the superelevation water surface mainly reflects on the centripetal acceleration, $(\bar{u}^2/h_1 h_2)$ $(\partial h_1/\partial \eta)$, i.e., the fifth term on the left-hand side of the transverse momentum equation. Hence, the variation in MaxH^* in region II can be ignored, and one only needs to focus on the variation in MaxU^*.

Justification on Dimensionless Parameters

To test the correlation between MaxU^* and the dimensionless parameters included in Eq. (12), the functional relationship of MaxU^* and these dimensionless parameters using a log–log scale is established as $\ln(\text{Max}U^*) = C_0 + \Sigma_{i=1} C_i \ln(D_i)$ with C_0 = constant; D_i = dimensionless parameter; and C_i = coefficient associated with D_i. The coefficients obtained by the regression analysis that are statistically significant are listed in Table 2. The results indicate that F has significant effect on MaxU^*. As far as shallow water flow model is concerned, F should be one of the most important parameters and has equal weight of the effect to the models. In other words, the difference of results simulated between models due to the F effect cannot apparently be distinguished. In addition, the main purpose of this study aims at investigating the velocity redistribution in a channel bend, rather than the gravitational force effect on the free surface flow. Hence, the effect of F can be removed hereafter. Yen (1965) found that the general features of secondary flow in a bend are independent of H/B as long as $H/B \ll 1$ in which the influence from the banks

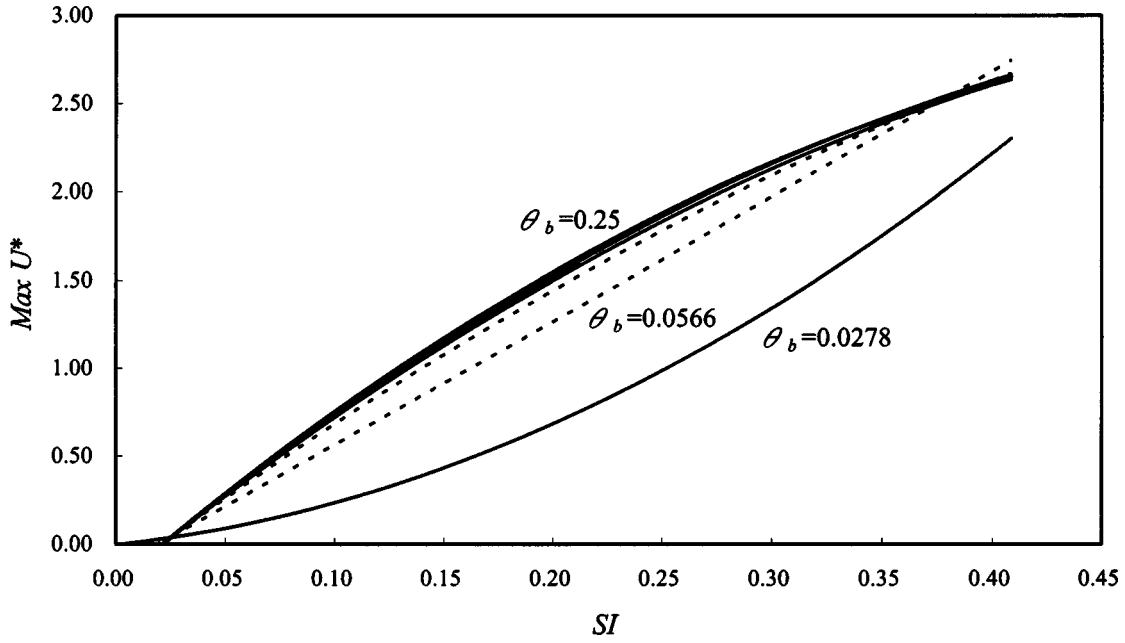

Fig. 3. Plot of regression functions of MaxU^* versus SI for various θ_b

J. Hydraul. Eng. 2003.129:597-612.

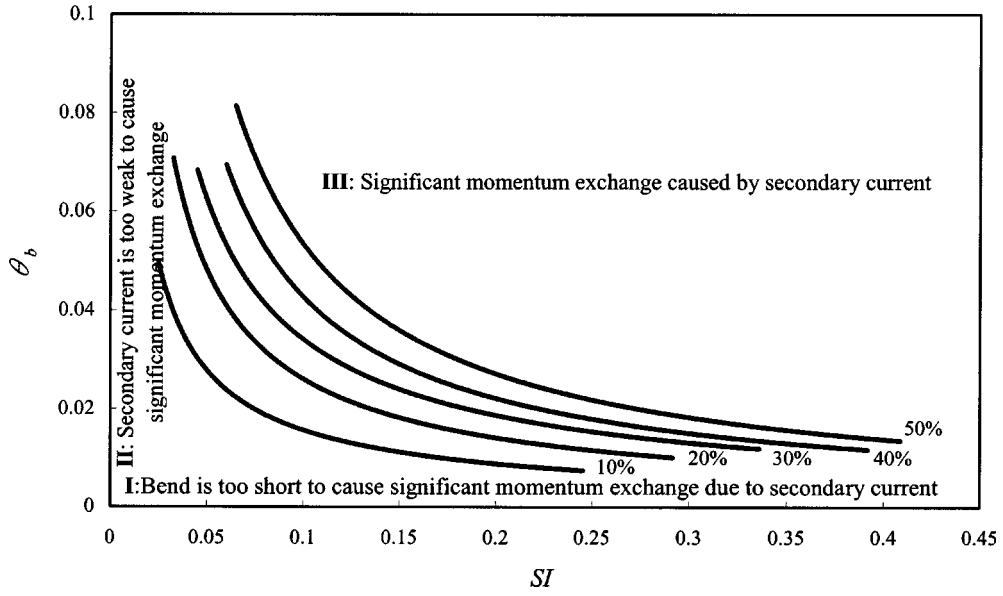

Fig. 4. Contours of MaxU^* as a function of SI and θ_b (MaxU^*–SI–θ_b relation)

or sidewalls can be neglected. Rozovskii (1961) also indicated that the wall effect could be neglected in the bends with small H/B values. In the present study, H/B for all the study cases are between 4.5×10^{-3} and 9.41×10^{-2} which are much smaller than 1. Therefore, the effect of H/B can be ignored. Table 3 shows the regression results, in which one can observe that SI has the most significant effect on MaxU^* and θ_b has the least, and the R^2 value is reduced from 0.938 to 0.904.

Table 5. Regression Functions of θ_b versus SI for Various MaxU^*

MaxU^*	Regression functions	R^2
0.1	$\theta_b=0.0023SI^{-0.8299}$	0.268
0.2	$\theta_b=0.0034SI^{-0.8852}$	0.288
0.3	$\theta_b=0.0046SI^{-0.8674}$	0.297
0.4	$\theta_b=0.0048SI^{-0.9463}$	0.350
0.5	$\theta_b=0.0057SI^{-0.9732}$	0.332

Effects of SI and θ_b on MaxU^*

Fig. 2 shows that for various θ_b, MaxU^* taken from the corresponding θ_b cross section is closely correlated to SI and its value increases as SI increases. A set of regression functions for MaxU^* and SI under various θ_b are presented in Table 4. Those regression functions with high R^2 values in Table 4 can be used to determine the MaxU^* values at various θ_b with known SI value. By judging the value of MaxU^*, users can, therefore, select the proper model for the bend-flow simulation.

Fig. 3 shows MaxU^* as a function of SI for various θ_b. From Fig. 3, one can observe that MaxU^* increases with θ_b for a fixed SI. The physical meaning behind the dependence of θ_b lies in the fact that secondary current in a channel bend is generated at the

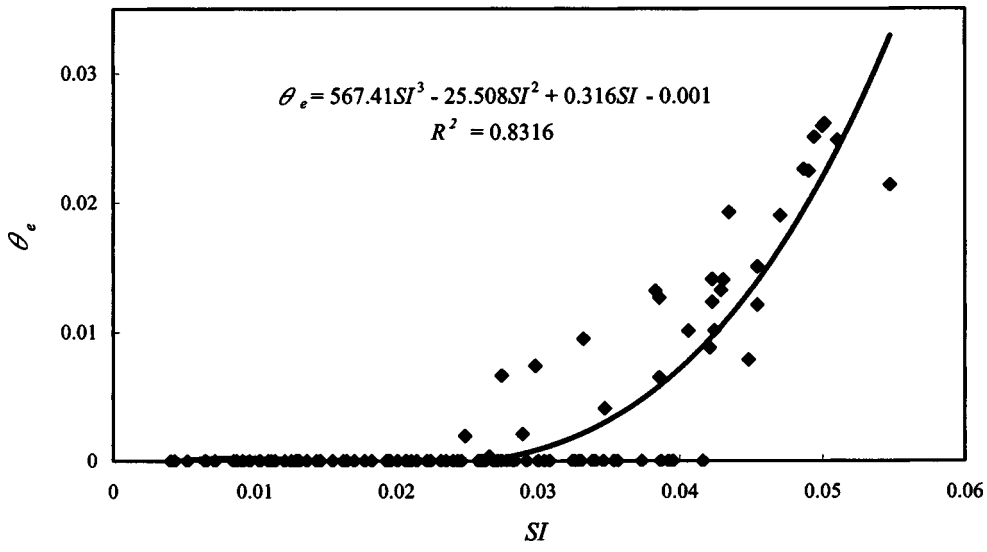

Fig. 5. Influence of SI on θ_e

J. Hydraul. Eng. 2003.129:597-612.

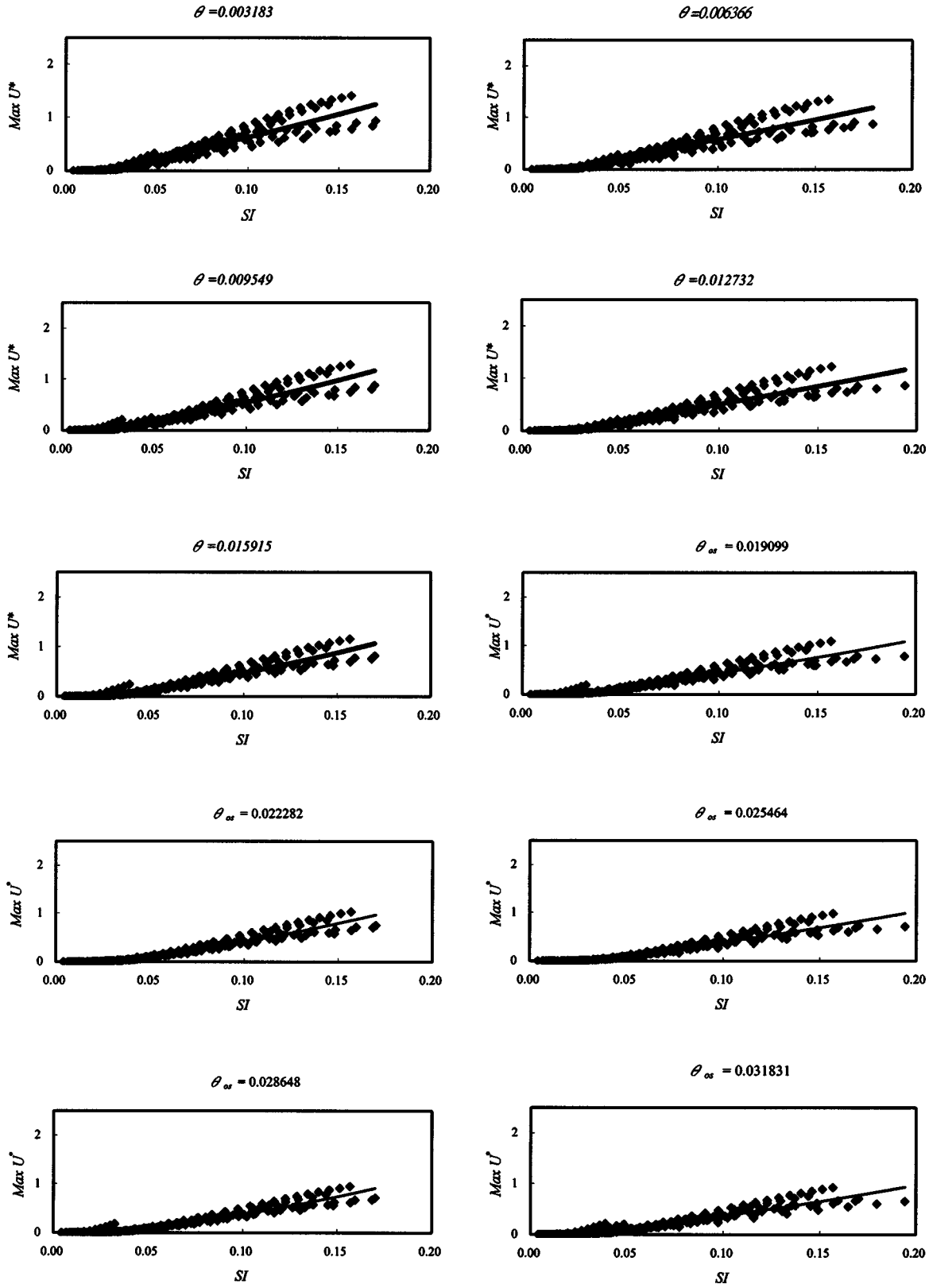

Fig. 6. MaxU^* as function of *SI* for various θ_{os}

bend entrance and the influence of secondary current needs a rather long distance to establish (de Vriend 1981). Therefore, the longitudinal velocity redistribution in the bend region also needs a rather long distance to reach its stable distribution. From Fig. 3, it clearly shows that near the entrance to the bend the change of MaxU^* grows much more rapidly than that away from the entrance to the bend for a fixed *SI*. Eventually, the change in MaxU^* gradually stabilizes as θ_b increases and $\theta_b = 0.25$ (i.e., 90° bend) seems to be a limiting case. When θ_b is greater than 0.25, the MaxU^*-SI relation remains almost identical. Furthermore, from Fig. 3, one can also observe that MaxU^* almost equals to zero when *SI* is less than 0.02. In other words, signifi-

J. Hydraul. Eng. 2003.129:597-612.

Table 6. Regression Functions of MaxU^* versus SI for Various θ_{os}

θ_{os}	Regression functions	R^2
0.003 183	$\text{Max}U^* = 6.6758SI^2 + 6.9976SI - 0.1417$	0.887
0.006 366	$\text{Max}U^* = 2.4937SI^2 + 6.971SI - 0.1443$	0.881
0.009 549	$\text{Max}U^* = 13.933SI^2 + 5.0865SI - 0.1017$	0.9
0.012 732	$\text{Max}U^* = 3.2772SI^2 + 6.0276SI - 0.1324$	0.891
0.015 915	$\text{Max}U^* = 16.488SI^2 + 3.9524SI - 0.0855$	0.911
0.019 099	$\text{Max}U^* = 7.2926SI^2 + 4.6431SI - 0.1008$	0.899
0.022 282	$\text{Max}U^* = 17.363SI^2 + 3.2171SI - 0.0796$	0.926
0.025 464	$\text{Max}U^* = 7.4424SI^2 + 4.1564SI - 0.102$	0.909
0.028 648	$\text{Max}U^* = 19.113SI^2 + 2.4235SI - 0.0559$	0.931
0.031 831	$\text{Max}U^* = 8.0995SI^2 + 3.6358SI - 0.0802$	0.904

cant momentum exchange due to secondary current would not occur while SI is less than 0.02.

Establishment of Max$U^*-SI-\theta_b$ *Relation*

One conclusion that can be drawn from the aforementioned analysis is that MaxU^* is mainly dependent of SI and θ_b. The relationship for some fixed MaxU^*, say 10, 20, 30, 40, and 50%, as a function of SI and θ_b (Max$U^*-SI-\theta_b$ relation) can be established as shown in Fig. 4. One can observe from Fig. 4 that SI is inversely proportional to θ_b for a fixed MaxU^*. The regression functions associated with the curves in Fig. 4 are presented in Table 5. This plot delineates the suitable application range of SI and θ_b for MaxU^* between the two models in channel bend and can be very useful for model selection.

The Max$U^*-SI-\theta_b$ relation shown in Fig. 4 may be classified into three regions, which are: Region I represents that the bend is too short to cause significant momentum exchange due to secondary current; region II represents that the secondary current is too weak to cause significant momentum exchange; and region III represents that the significant momentum exchange is caused by secondary current. Based on the acceptable MaxU^* required by the users, one can easily demarcate the border between region I (or II) and III. Near region I or II, the momentum exchange caused by the secondary current is not significant so that the conventional model, therefore, may be appropriate for the bend-flow problem. As the condition falls in region III, the secondary-current effect in a given bend can no longer be ignored. Then, the bend-flow model should be the better choice.

Flow in Straight Portion Following Bend

Justification on Dimensionless Parameters

Again, as pointed out by Nouh and Townsend (1979), the residual effect of secondary current in the straight channel following a bend continues to influence the flow field for a significant distance downstream from the bend exit. The longitudinal velocity in a straight reach beyond a bend needs a rather long distance to reach its straight channel distribution, which is uniform along the channel width (Rozovskii 1961; de Vriend 1978). Hence, the rate of decay of the secondary current existing in the straight channel portion needs a bend to be considered. Nouh and Townsend (1979) assumed that the effective length of the straight channel following the bend (L_e), within which the decay process takes place, is equivalent to the length measured from the bend exit to a point downstream where residual secondary-current intensity is to be 10% of the initial intensity measured at the bend exit. Based on this criterion, Nouh and Townsend (1979) simply neglected the transverse pressure gradient and gave an expression that L_e should depend on bottom roughness and water depth. Struiksma et al. (1985) proposed that if there is no secondary flow, L_e should depend on bottom roughness and water depth. Kalkwijk and Booij (1986) assumed that the mean velocity and radius of curvature are constant along a streamline and gave an expression that L_e should depend on bottom roughness and water depth. de Vriend (1981) deduced that the velocity profile in the transverse direction at the bend exit should depend on the radius of curvature and gave an expression that L_e depends on Reynolds number and water depth. However, de Vriend ignored the parameter of the radius of curvature after the bend exit.

Since velocity in the vertical direction cannot be simulated by 2D depth-averaged models, the present analyses cannot express the decay of the secondary current in the straight channel portion

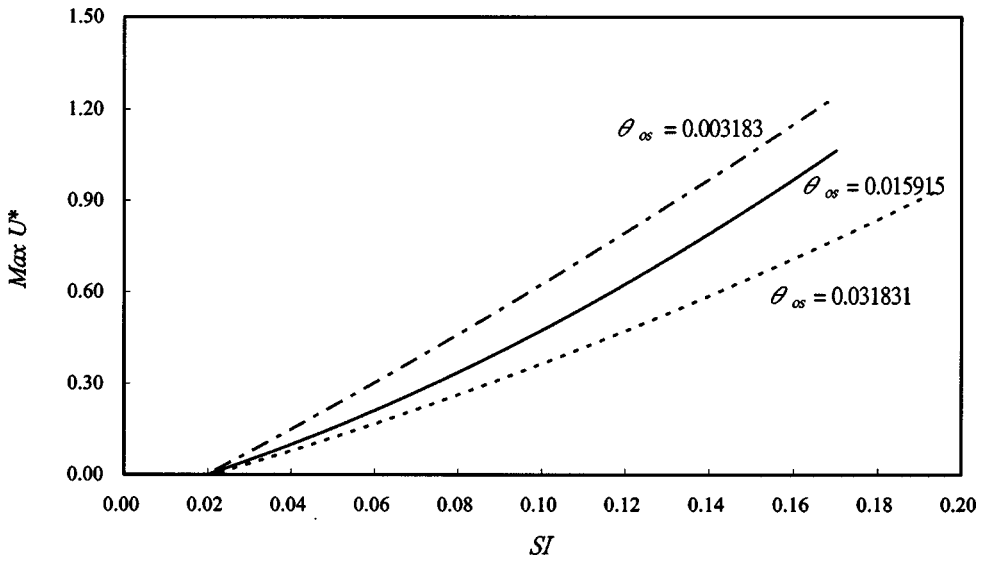

Fig. 7. Plot of regression functions of MaxU^* versus SI for various θ_{os}

J. Hydraul. Eng. 2003.129:597-612.

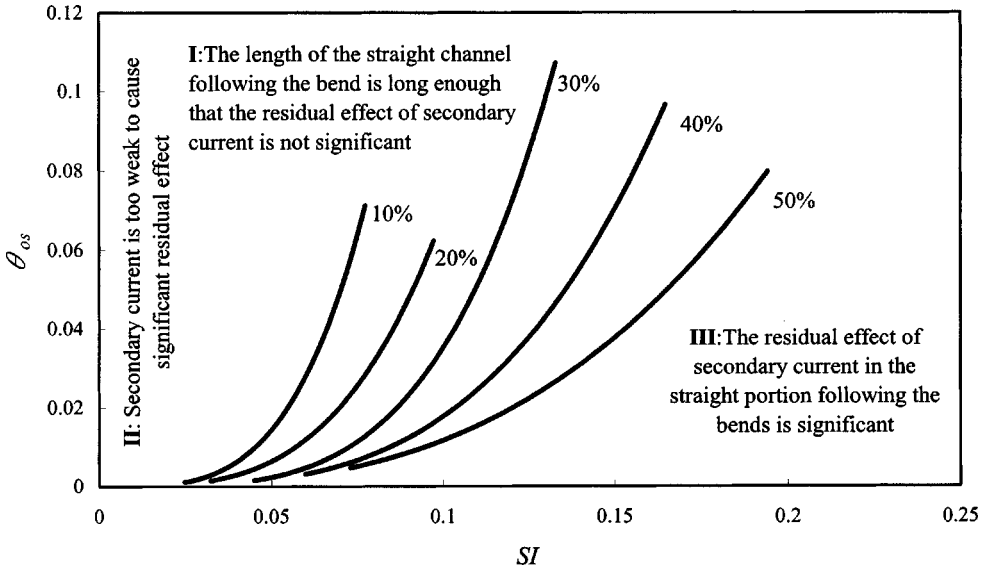

Fig. 8. Contours of MaxU^* as function of SI and θ_{os} (Max$U^*-SI-\theta_{os}$ relation)

following a bend. Eventually, the longitudinal velocity after L_e would gradually reach the same distribution in straight channel. Hence, a newly L_e is adopted herein which is equivalent to the length measured from the bend exit to a cross section downstream where $\text{Max}(|\bar{u}^b-\bar{u}^b_m|/\bar{u}^b_m)<0.1$ in which $\bar{u}^b_m$ = averaged cross-sectional longitudinal velocity of the bend-flow model; and $\bar{u}^b$ = longitudinal velocity from the bend-flow model at each grid point in the specified cross section. Fig. 5 presents the simulated results of the dimensionless effective length of straight channel following the bend ($\theta_e=L_e/(2\pi r_c)$) as a function of SI. It shows that θ_e is closely related to and increases with SI.

The regression analysis is performed to examine the correlation between MaxU^* and the dimensionless parameters included in Eq. (12) using a log–log scale. The results of the regression analysis in the straight portion following the bend are similar to those in the channel-bend region. The key parameters related to MaxU^* in the straight portion following the bend would also be the same parameters as those in the channel-bend region, including SI and θ_{os}.

Effects of SI and θ_{os} on MaxU^*

In the straight channel portion following a bend, both the conventional and bend-flow models have the same governing equations. The difference between the two will be caused by the flow condition at the bend exit which is the intersection between the end of the bend and the following straight channel. As can be observed from Fig. 2, the discrepancy of the flow condition between the models at the bend exit, which is $\theta_b=0.25$, mainly depends on SI. It would be expected that larger values of SI would associate with high MaxU^*. Fig. 6 shows that for various θ_{os}, MaxU^* taken from the corresponding θ_{os} cross section has a close increasing relation with SI. The regression functions of MaxU^* and SI for various θ_{os} presented in Table 6 show high R^2 values which indicate that Fig. 6 (or Table 6) can be used as a guideline to justify whether or not the bend-flow model is needed to reflect the proper flow condition at the entrance to the straight portion following a bend.

The relationships between MaxU^* and SI for three values of θ_{os} are shown in Fig. 7 from which one can observe that MaxU^* decreases as θ_{os} increases for a fixed SI. This can be interpreted as that the residual effect of secondary current continues to influence the flow field after the bend exit section and this effect needs a rather long distance to scatter. Furthermore, from Fig. 7, one can find that MaxU^* almost equals zero when SI is less than 0.02. This implies that significant residual effect of secondary current in the straight portions following a bend would not take place while SI is less than 0.02.

Table 7. Regression Functions of θ_{os} versus SI for Various MaxU^*

MaxU^*	Regression functions	R^2
0.1	$\theta_{os}=861.95SI^{3.6739}$	0.499
0.2	$\theta_{os}=181.72SI^{3.4248}$	0.669
0.3	$\theta_{os}=298.17SI^{3.9289}$	0.566
0.4	$\theta_{os}=44.556SI^{3.4009}$	0.616
0.5	$\theta_{os}=7.6412SI^{2.8168}$	0.601

Establishment of Max$U^*-SI-\theta_{os}$ Relation

From the aforementioned analyses, it is clear that MaxU^* increases as SI increases or θ_{os} decreases. The relationship for some fixed MaxU^* as a function of SI and θ_{os} (Max$U^*-SI-\theta_{os}$ relation) can be established as in Fig. 8. The regression functions corresponding to the curve in Fig. 8 are presented in Table 7. The Max$U^*-SI-\theta_{os}$ relation shown in Fig. 8 indicates that for a given small value of SI (say less than about 0.1), MaxU^* might drop dramatically as θ_{os} grows initially for a short range. While θ_{os} keeps increasing, the rate of decay of MaxU^* decreases and, eventually, may remain at a constant value. This means that the secondary current effect will influence the flow field significantly for a short distance following the bend exit but may stay a minor effect for very long and never dissipate at all. As SI increases the decay rate of MaxU^* will slow down and the influence of secondary current will last longer. For sure, for very small SI approaching null, the secondary-current effect becomes very weak and negligible.

Similar to Fig. 4, the Max$U^*-SI-\theta_{os}$ relation shown in Fig. 8 can be classified into three regions, which are: Region I represents

J. Hydraul. Eng. 2003.129:597-612.

Table 8. Channel Dimensions and Flow Conditions for de Vriend and Koch's Experiments

Experimenter	Discharge Q (m^3/s)	Mean depth H (m)	Mean velocity U (m/s)	Channel width B (m)	Bend radius r_c (m)	H/B	d/r_c	Chezy factor c ($m^{1/2}/s$)	Slope	F	**R** ($\times 10^4$)	SI
de Vriend and Koch I (1977)	0.305	0.25	0.2	6	50	0.0417	0.005	50	0.0003	0.13	4.6	0.0798
de Vriend and Koch II (1977)	0.61	0.25	0.4	6	50	0.0417	0.005	70	0.0003	0.26	9.2	0.1117

that the length of the straight channel following a bend is long enough that the secondary-current effect at the bend exit is not important; region II represents that the secondary-current effect at the bend exit is too weak to cause significant residual effect; and region III represents that the secondary-current effect at the bend exit is important. Again, similar to the consequence abstracted in Fig. 4, based on the acceptable MaxU^* required by the users, one can easily demarcate the border between region I (or II) and III. Near region I or II, the residual effect of secondary current is not obvious. Therefore, the conventional model may also solve the bend-flow problem properly. As the condition falls in region III, the residual effect of secondary current can no longer be ignored. Then, the bend-flow model should be the better one.

Application and Verification of Max$U^*-SI-\theta$ Relation

The experimental data conducted by de Vriend and Koch (1977) is adopted herein to demonstrate how to use the proposed Max$U^*-SI-\theta$ relation shown in Figs. 4 and 8 and the regression functions shown in Figs. 3 and 7. Through the comparison with the model simulation and measured results, the proposed relation has been verified. Data regarding the channel dimensions and flow conditions are summarized in Table 8.

Description of Data Simulated

In de Vriend and Koch's experiment, the channel consisted of a 39 m long straight section followed by a 90° bend with a radius of curvature of 50 m. The channel cross section was rectangular, and the width was 6 m. The channel bed was horizontal in the straight part and had a slope of 3×10^{-4} in the curved part. Two series of measurements were carried out, one with a discharge 0.305 m^3/s (case I), and the other one with a discharge of 0.610 m^3/s (case II). The Chezy factors were 50 $m^{1/2}/s$ and 70 $m^{1/2}/s$, respectively. In addition, the mean flow depth was 0.25 m for both experiments; yielding mean velocities of about 0.2 m/s and 0.4 m/s, respectively. SI were 0.0798 and 0.1117, respectively.

The mesh of 113×35 was used in the simulation. The simulation reach covered a 23 m long straight channel before the entrance of the bend and a 90° bend with a radius of curvature of 50 m. The upstream boundary condition was the inflow discharge, the downstream boundary condition was the measured water surface elevation and no-slip boundary was used at the banks.

Results and Discussions

For this experiment, no data have been measured along the straight portion following a bend. Hence, only the results for the channel-bend region are demonstrated and verified. As shown in Fig. 9, one can clearly demarcate the border between region I (or II) and III when 50% error, for instance, is considered as the acceptable MaxU^*. The θ_b value at the border can be determined from the known SI value, which are $\theta_b=0.067$ and 0.048 for cases I and II, respectively. Hence, for a channel-bend curvature less than these θ_b values, results computed from both the conven-

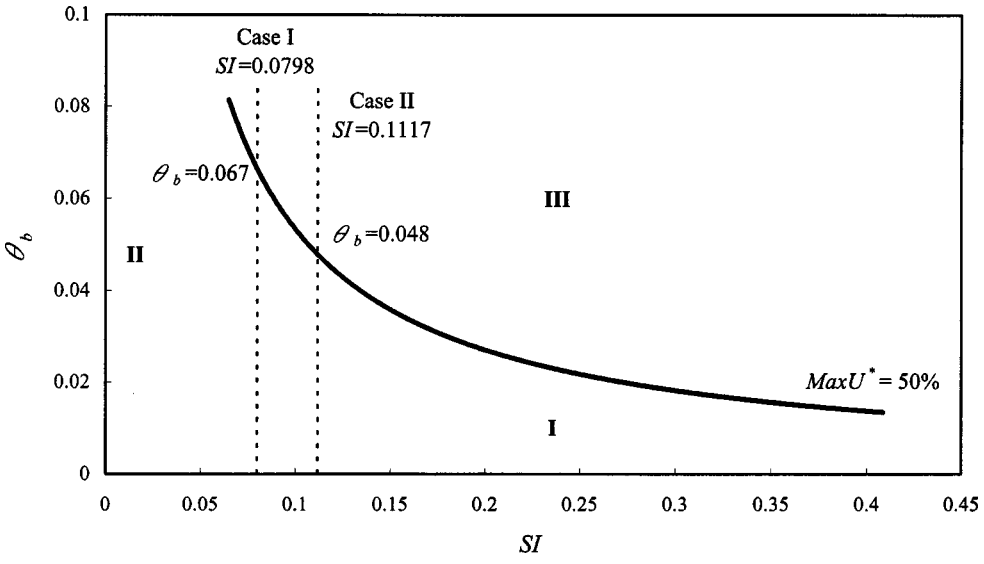

Fig. 9. Use of Max$U^*-SI-\theta_b$ relation for de Vriend and Koch's experimental data

J. Hydraul. Eng. 2003.129:597-612.

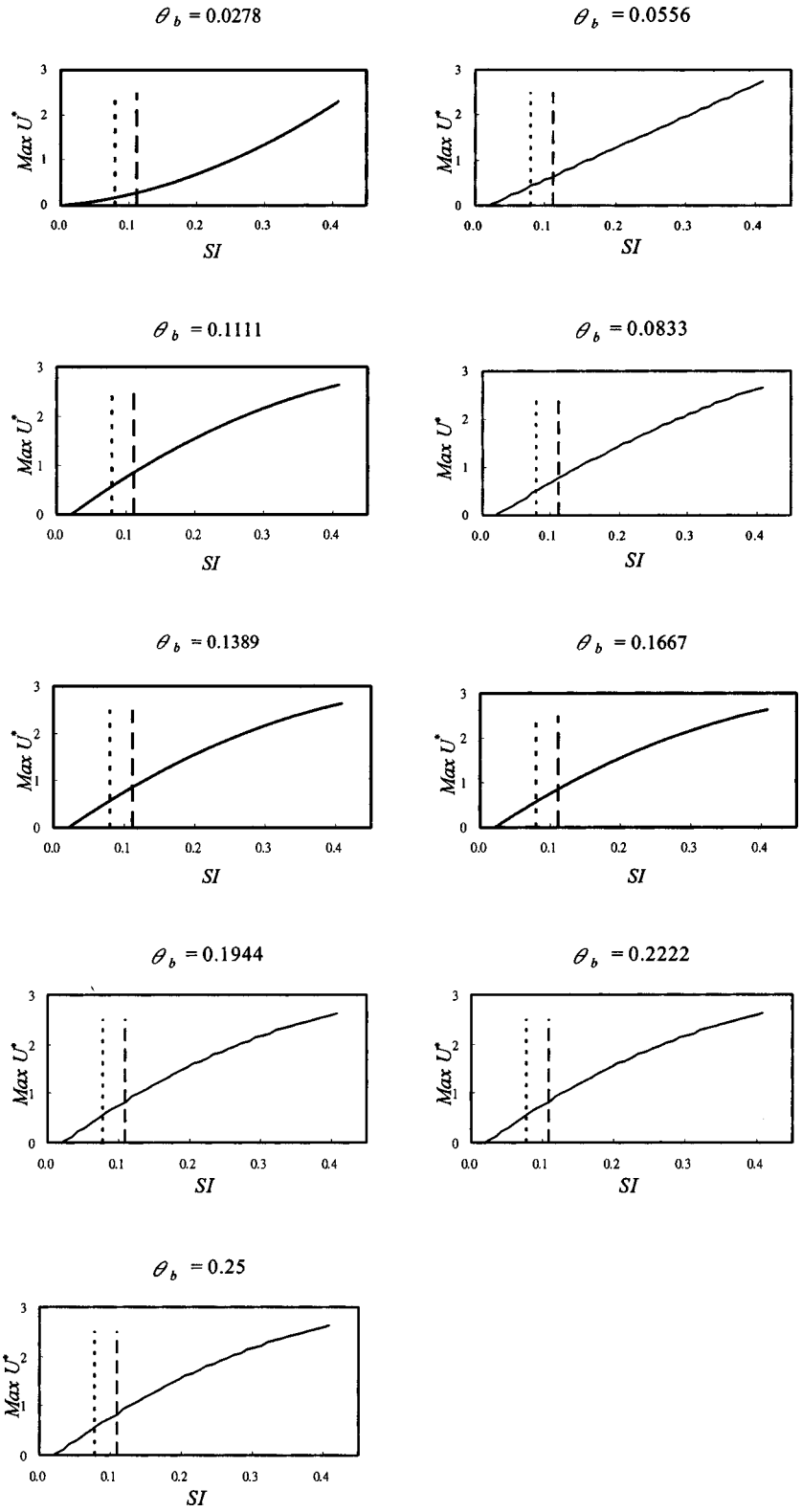

Fig. 10. Use of the regression functions in channel-bend region for de Vriend and Koch's experimental data. Case I (– – –); case II (——).

tional and bend-flow models will be considered acceptable. On the other hand, for the region with greater θ_b, the bend-flow model should be used.

As shown in Fig. 10, the MaxU^* values at various θ_b can be obtained from the known *SI* value. The MaxU^* values are greater than 50% for all cases except case I with $\theta_b = 0.0278$ and 0.0556 and case II with $\theta_b = 0.0278$. At the bend exit, that is $\theta_b = 0.25$, the MaxU^* values of cases I and II reach about 57% and 86%, respectively. The results imply that even with 50% error tolerance, the conventional model can only be suitable for a certain short range of channel bend, that is, about less than 24° and 17° of the bend for cases I and II, respectively. From Figs. 9 and 10,

J. Hydraul. Eng. 2003.129:597-612.

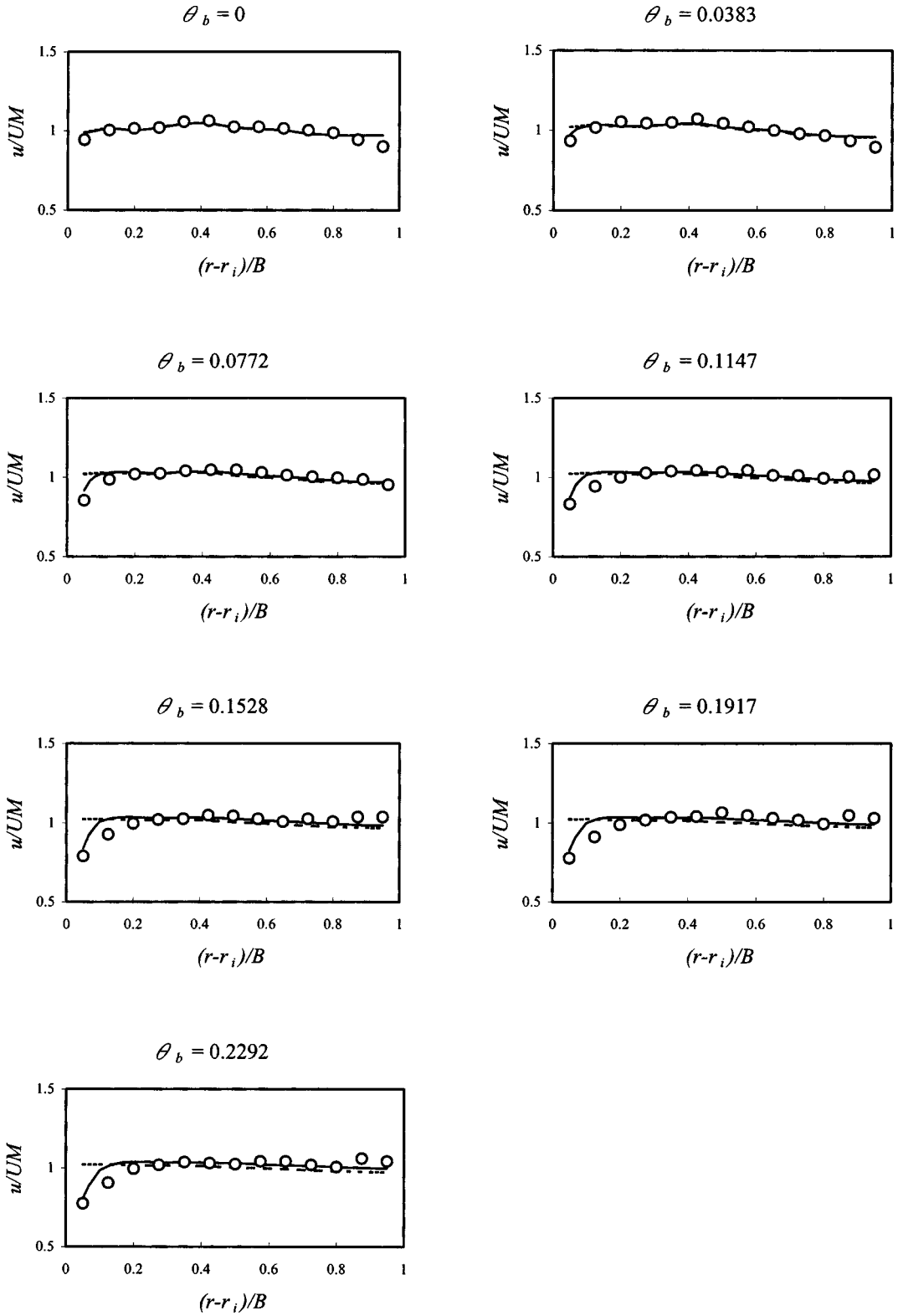

Fig. 11. Velocity ratio u/UM across dimensionless channel width for the simulation of case I of de Vriend and Koch's experiment. Measured (○); bend-flow model (—); and conventional model (···).

one may conclude that for the cases of de Vriend's experiment, the bend-flow model should be a better choice.

In order to verify the proposed Max$U^*-SI-\theta$ relation, numerical simulations for the experimental data were performed by both models. Figs. 11 and 12 show the variation of velocity ratios u/UM across the dimensionless channel width $[(r-r_i)/B]$ obtained from the bend-flow model, the conventional model, and the measured data for cases I and II, respectively, in which u = depth-averaged longitudinal velocity; UM = cross section averaged longitudinal velocity; and r_i = radius of curvature of the inner bank. From Figs. 11 and 12, it is clear that the longitudinal velocity distributions at the bend entrance are identical for both

J. Hydraul. Eng. 2003.129:597-612.

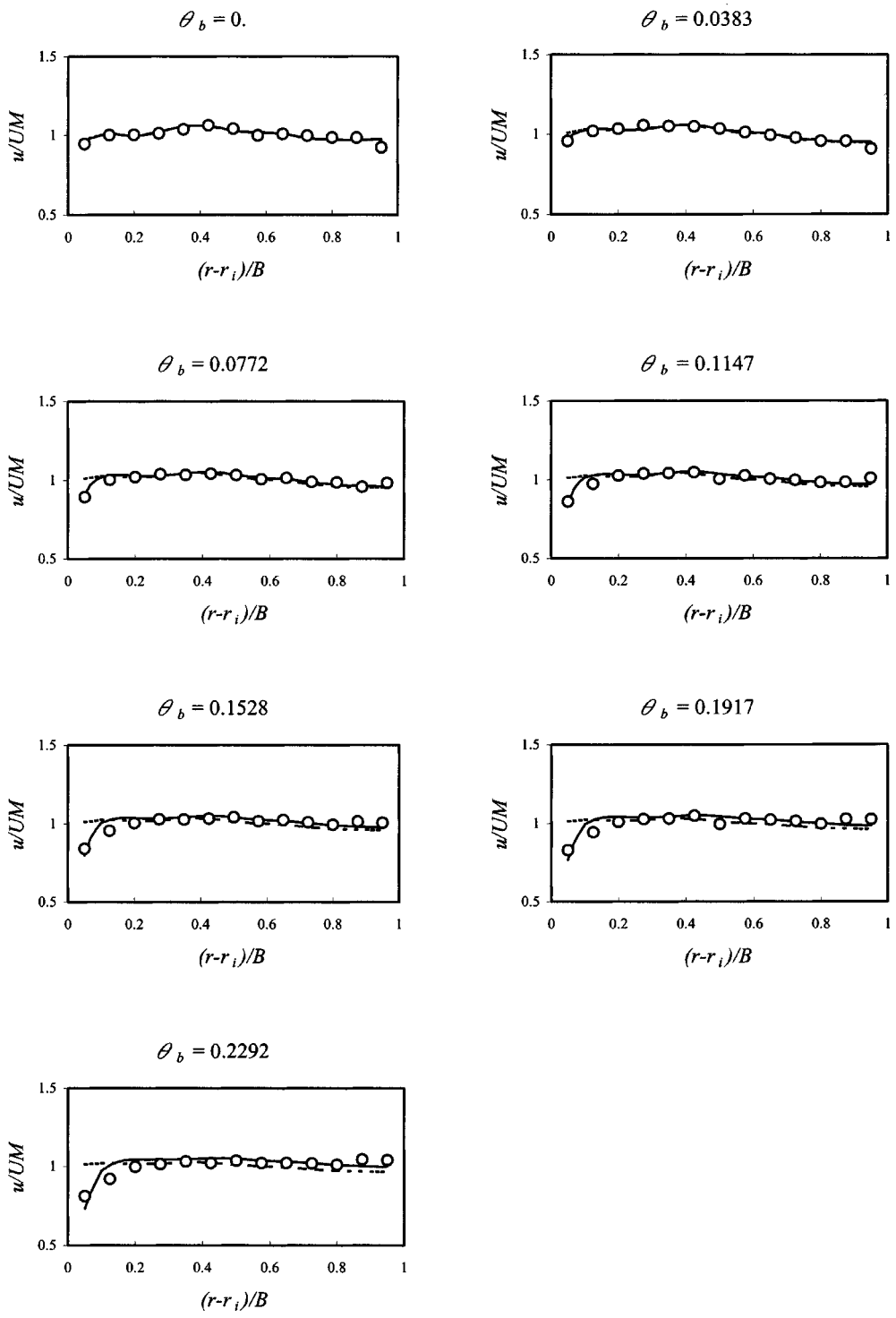

Fig. 12. Velocity ratio u/UM across dimensionless channel width for the simulation of case II of de Vriend and Koch's experiment. Measured (○); bend-flow model (—); and conventional model (···).

models. After the bend entrance, one can observe that the simulation results by the bend-flow model have fairly good agreement with measured data in which the longitudinal velocity near the outer bank increases along the bend and becomes greater than that near the inner bank due to the transverse convection of longitudinal momentum along the bend caused by the secondary current. On the other hand, the results simulated by the conventional model are consistent with the potential theory in which the longitudinal velocity is inversely proportional to the radius of the curvature. The inaccuracy of longitudinal velocity distribution with measured data is generated at the entrance to the bend and increases along the channel bend when the conventional model is adopted. Figs. 11 and 12 clearly illustrate the need of the bend-flow model for simulating the de Vriend and Koch's experiments. This result is consistent with the analysis previously made on the basis of the proposed $\mathrm{Max}U^*-SI-\theta$ relation.

J. Hydraul. Eng. 2003.129:597-612.

Conclusions

A numerical experiment on the suitability of 2D depth-averaged models for bend-flow simulation is presented in this paper. Two commonly used 2D depth-averaged models, i.e., a bend-flow model and a conventional model, were considered. The applicability of each model has been analyzed by examining the maximum relative differences of longitudinal velocity MaxU^*. The regression analysis shows that MaxU^* mainly depends on the relative strength of secondary current *SI* and the relative length of channel (θ_b or θ_{os}); and the effect of *SI* is much more evident. The momentum exchange due to secondary current in the channel bend and its residual effect in the straight channel portion following a bend would not be significant when *SI* is less than 0.02. A useful relation MaxU^*–SI–θ_b given in Fig. 4 and MaxU^*–SI–θ_{os} given in Fig. 8, has been established which serves as a guideline for model users to distinguish whether the bend-flow model is needed or not to capture the secondary-current effect along the channel-bend region and to reflect the proper flow condition at the entrance to the straight portion following a bend. The verification of the functional relation proposed has been carried out with the use of the experimental data conducted by de Vriend and Koch (1977) and it shows very convincing results.

Acknowledgments

Partial financial support of this study from the National Science Council of Taiwan, R.O.C., through Contract NSC-89-2211-E009-031 is greatly appreciated. The computer resources used in this study were provided by the National High-Performance Computing Center in Taiwan, R.O.C.

Notation

The following symbols are used in this paper:

B = channel width;
$C_f = g/c^2$ = friction factor;
C_i = regression coefficient associated with D_i;
C_0 = constant;
c = Chezy factor;
D_i = dimensionless parameter;
d = water depth;
F = Froude number;
g = gravitational acceleration;
H = mean flow depth;
h_1 and h_2 = metric coefficients in ξ and η directions, respectively;
k = von Karman's constant;
L = channel length;
L_b = bend length;
L_e = effective length of straight channel following bend;
L_{os} = outlet straight channel length;
MaxH^* = maximum relative difference in depth;
MaxU^* = maximum relative difference in longitudinal velocity;
MaxV^* = maximum relative difference in transverse velocity;
n = Manning's roughness coefficient;
R = Reynolds number;
r = radius of curvature;
r_c = centerline radius of curvature;
SI = relative strength of secondary current;
S_0 = channel slope;
$T_{i,j}$ = integrated effective stress;
t = time;
U = ξ components of mean velocity;
u = ξ components of velocity;
u_* = shear velocity;
V = η components of mean velocity;
v = η components of velocity;
z_b = bed elevation;
z_s = water surface elevation;
Δ = difference between conventional model and bend-flow model;
$\zeta = (z - z_b)/d$ = dimensionless distance from bed;
θ = relative length of channel;
θ_b = relative length of bend;
θ_e = dimensionless effective length of straight channel following bend;
θ_{os} = relative length of outlet straight channel;
ν_l = laminar kinematic viscosity;
ν_t = turbulent kinematic viscosity;
μ = viscosity;
ξ and η = orthogonal curvilinear coordinates in streamwise axis and transverse axis, respectively;
ρ = fluid density;
τ_{b1}, τ_{b2} = ith direction components of free-surface and bed-shear stress, respectively; and
$\tau_{i,j}$ = shear stress acting on face perpendicular to i-axis and acting in direction of j-axis.

Superscripts

b = dependent variables from bend-flow model;
$n+1$ = unknown variables at time level $(n+1)$;
$n+1/2$ = provisional variables between steps;
$(-)$ = time average;
$(=)$ = depth average; and
$(')$ = fluctuating component.

Subscripts

b = dependent variables at channel bed; and
s = dependent variables at water surface.

References

Chang, Y. C. (1971). "Lateral mixing in meandering channels." PhD dissertation, Iowa Institute of Hydraulic Research, Univ. of Iowa, Iowa City, Iowa.

de Vriend, H. J. (1977). "A mathematical model of steady flow in curved shallow channels." *J. Hydraul. Res.*, 15(1), 37–54.

de Vriend, H. J. (1978). "Developing laminar flow in curved rectangular channels." *Internal Rep. No. 6-78*, Dept. of Civil Engineering, Laboratory of Fluid Mech., Delft Univ. of Technology, Delft, The Netherlands.

de Vriend, H. J. (1981). "Steady flow in shallow channel bends." *Communications on Hydraulics*, Delft Univ. of Technology, Dept. of Civil Engineering, Delft, The Netherlands, *Rep. No. 81-3*.

de Vriend, H. J., and Geldof, H. J. (1983). "Main flow velocity in short river bends." *J. Hydraul. Eng.*, 109(7), 991–1011.

de Vriend, H. J., and Koch, F. G. (1977). "Flow of water in a curved open channel with a fixed plan bed." *Report on Experimental and Theoretical Investigations*, *Rep. No. R675-VM1415*, Part I, Delft Univ. of

J. Hydraul. Eng. 2003.129:597-612.

Technology, Delft, The Netherlands.
Falcon, A. M. (1979). ''Analysis of flow in alluvial channel bends.'' PhD thesis, Dept. of Mechanical and Hydraulic Engineering, Univ. of Iowa, Iowa City.
Finnie, J., Donnell, B., Letter, J., and Bernard, R. S. (1999). ''Secondary flow correction for depth-averaged flow calculations.'' *J. Hydraul. Eng.*, 125(7), 848–863.
Flokstra, C. (1977). ''The closure problem for depth-averaged two-dimensional flows.'' *Proc., 18th Congress of the Int. Association for Hydraulic Research*, 247–256.
Kalkwijk, J. P. T., and Booij, R. (1986). ''Adaptation of secondary flow in nearly-horizontal flow.'' *J. Hydraul. Res.*, 24(1), 19–37.
Kalkwijk, J. P. T., and de Vriend, H. J. (1980). ''Computation of the flow in shallow river bends.'' *J. Hydraul. Res.*, 18(4), 327–342.
Leschziner, M. A., and Rodi, W. (1979). ''Calculation of strongly curved open channel flow.'' *J. Hydraul. Div., Am. Soc. Civ. Eng.*, 105(10), 1297–1314.
Lien, H. C., Hsieh, T. Y., Yang, J. C., and Yeh, K. C. (1999a). ''Bend-flow simulation using 2D depth-averaged model.'' *J. Hydraul. Eng.*, 125(10), 1097–1108.
Lien, H. C., Hsieh, T. Y., and Yang, J. C. (1999b). ''Use of two-step split-operator approach for 2D shallow water flow computation.'' *Int. J. Numer. Methods Fluids*, 30, 557–575.
Meselhe, E. A., and Sotiropoulos, F. (2000). ''Three-dimensional numerical model for open-channels with free surface.'' *J. Hydraul. Res.*, 38(2), 115–125.
Molls, T., and Chaudhry, M. H. (1995). ''Depth-averaged open-channel flow model.'' *J. Hydraul. Eng.*, 121(6), 453–465.
Nagata, T., Hosoda, T., Muramoto, Y., and Rahman, M. M. (1997). ''Development of the numerical model to forecast the channel processes with bank erosion.'' *Proc., 4th Japan-Chinese (Taipei) Joint Seminar on Natural Hazard Mitigation*, 167–176.
Nouh, M. A., and Townsend, R. D. (1979). ''Shear-stress distribution in stable channel bends.'' *J. Hydraul. Div., Am. Soc. Civ. Eng.*, 105(10), 1233–1245.
Odgaard, A. J. (1989). ''River-meander model. I: Development.'' *J. Hydraul. Eng.*, 115(11), 1433–1450.
Rastogi, A. K., and Rodi, W. (1978). ''Prediction of heat and mass transfer in open channels.'' *J. Hydraul. Div., Am. Soc. Civ. Eng.*, 104(3), 397–420.
Rozovskii, I. L. (1961). *Flow of water in bends of open channels*, The Israel Program for Scientific Translations, Jerusalem.
Sinha, S. K., Sotiropoulos, F., and Odgaard, A. J. (1998). ''Three-dimensional numerical model for flow through natural rivers.'' *J. Hydraul. Eng.*, 124(1), 13–24.
Struiksma, N., Olesen, K. W., Flokstra, C., and de Vriend, H. J. (1985). ''Bed deformation in curved alluvial channels.'' *J. Hydraul. Res.*, 23(1), 57–79.
Wu, W., Rodi, W., and Wenka, T. (2000). ''3D numerical modeling of flow and sediment transport in open channels.'' *J. Hydraul. Eng.*, 126(1), 4–15.
Ye, J., and McCorquodale, J. A. (1997). ''Depth-averaged hydrodynamic model in curvilinear collocated grid.'' *J. Hydraul. Eng.*, 123(5), 380–388.
Yen, B. C. (1965). ''Characteristics of subcritical flow in a meandering channel.'' *Rep. No. G-18988*, Institute of Hydraulic Research, Univ. of Iowa, Iowa.
Yen, C. L., and Ho, S. Y. (1990). ''Bed evolution in channel bends.'' *J. Hydraul. Eng.*, 116(4), 544–562.

J. Hydraul. Eng. 2003.129:597-612.